In *An Introduction to the Geometry and Topology of Fluid Flows* (ed. R.L. Ricca), 203-228.
NATO ASI Series: Mathematics. Kluwer, Dordrecht, The Netherlands (2001).

GEOMETRIC AND TOPOLOGICAL ASPECTS OF VORTEX MOTION

RENZO L. RICCA
Department of Mathematics
University College London
Gower Street, London WC1E 6BT, UK
E-mail: *ricca@math.ucl.ac.uk*

Abstract. In this paper we review some results on geometric and topological vortex dynamics. After some background on flow maps, topological equivalence of frozen fields and conservation laws, we discuss geometric aspects of vortex filament motion (intrinsic equations, connections with integrable dynamics and extension to higher dimensional manifolds) and the topological interpretation of kinetic helicity in terms of linking numbers. We recall basic results on evolution of vortex knots and links and outline possible applications of algebraic, geometric and topological measures to evaluate structural complexity of vortex flows.

1. Flow Maps and Topological Equivalence of Frozen Fields

Let $\mathcal{D}$ denote a fluid domain in $\mathbb{R}^3$, that is an open, unbounded, singly connected region of the Euclidean, three-dimensional space. The domain is filled by a homogeneous, inviscid fluid, which is treated as a mathematical continuum (i.e. neglecting microscopic and dissipative effects). Of course this is a mathematical simplification of reality, justified by assuming that the typical evolution time of the corresponding real process is much greater than the dissipative and diffusive characteristic time.

Fluid motion determines a continuous time-dependent re-arrangement of fluid regions in $\mathcal{D}$. We assume that fluid particles move with a velocity $\mathbf{u} = \mathbf{u}(\mathbf{x}, t)$, smooth function of the position vector $\mathbf{x}$ and time t, satisfying

$$\nabla \cdot \mathbf{u} = 0 \quad \text{in } \mathcal{D} \, ; \qquad \mathbf{u} = 0 \quad \text{as } \mathbf{x} \to \infty \, , \tag{1}$$

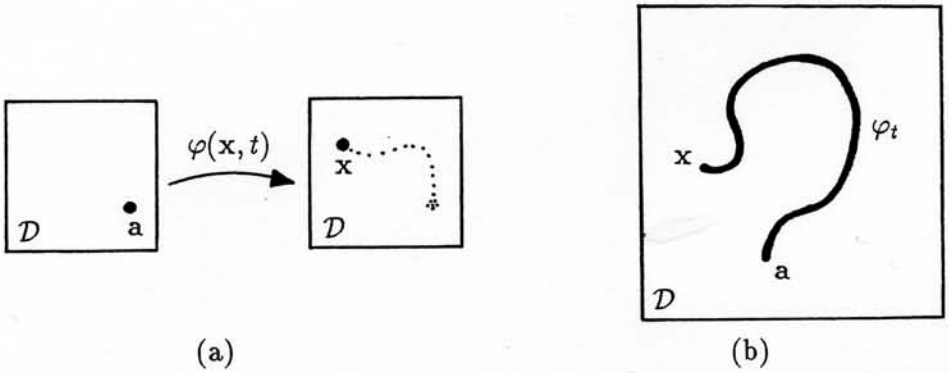

Figure 1. (a) A fluid particle moves in $\mathcal{D}$ by the action of a flow map φ associated with the fluid velocity $\mathbf{u}$; (b) as t varies, the collection of φ_t determines the trajectory followed by the fluid particle in time.

and that fluid motion is governed by the Euler equations

$$\frac{\partial \mathbf{u}}{\partial t} + (\mathbf{u} \cdot \nabla)\mathbf{u} = -\nabla p \, . \tag{2}$$

The velocity field $\mathbf{u}$ induces a map $\varphi = \varphi(\mathbf{x}, t)$ that at each time sends the fluid particle from the initial position $\mathbf{a}$ and time t_0 to the position $\mathbf{x}$ and time t: $\varphi_t : \mathbf{a} \to \mathbf{x}$, $\forall t \in I$ (I finite). Since this map advances each fluid particle from $\mathbf{a}$ to $\mathbf{x}$, as t varies the collection of φ_t determines the *particle path* followed by the fluid particle in time (see Figure 1).

We have:

Definition 1.1 *A* **fluid flow map** *is a functional element $\varphi \in \Phi$, where*

$$\Phi \equiv \left\{ C^\nu : \exists \varphi^{-1} \,|\, \mathbf{a} = \varphi^{-1}(\mathbf{x}, t) \, \forall t \in I; \; \varphi \textit{ volume-preserving} \right\} \, , \tag{3}$$

where Φ is a differential manifold of infinite dimension and C^ν denotes the class of functions continuously differentiable of order ν.

For obvious reasons we may want to take $\nu \geq 3$. Under the action of φ any portion of $\mathcal{D}$ will move in the fluid while changing shape, but keeping volume constant.

Remark 1.2 In this paper we concentrate on *non-degenerate* ('tame') flow maps, i.e. flow maps that are single-valued and continuous everywhere. Flow patterns exhibiting cusp formation, bifurcations and other types of physical singularities are actually ubiquitous in nature; however, we need to develop appropriate mathematical descriptions to be able to include these type of 'degeneracies' in a comprehensive mathematical theory of fluid flows.

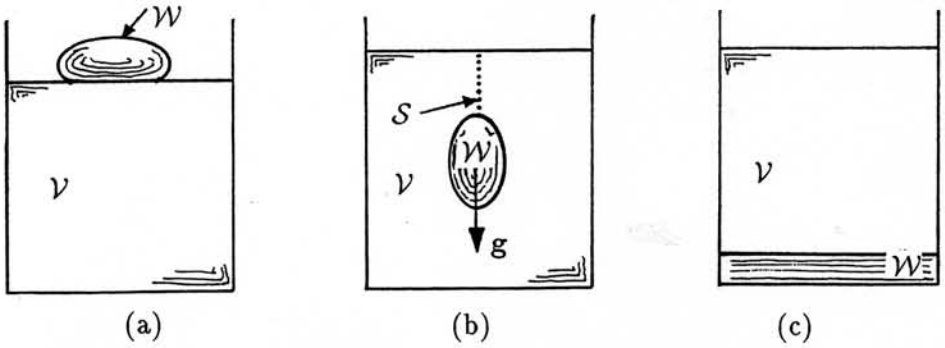

Figure 2. (a) A box is filled by some fluid in $\mathcal{V}$ with a blob of denser fluid in $\mathcal{W}$. Initially the two fluids are at rest; (b) under the action of the gravitational force $\mathbf{g}$ the fluid in $\mathcal{W}$ starts gradually to sink and penetrate $\mathcal{V}$, leaving behind a subset of 'virtual' separation $\mathcal{S}$ (dotted line). (c) As $t \to \infty$ the denser fluid precipitates to the bottom surface of the box.

Example 1.3 [Degenerate flow maps] A box is filled by two different fluids: one fluid occupies a region $\mathcal{V}$ and a blob of denser fluid is concentrated in $\mathcal{W}$, floating on top of $\mathcal{V}$ (see Figure 2a). Suppose that the two fluids have different, high surface tension, providing strong coherency of the bounding surfaces (so as to avoid mixing). The two fluid system is initially at rest, but is subject to a uniform gravitational field $\mathbf{g}$. Since gravity pulls down the blob of denser fluid, $\mathcal{W}$ starts gradually to deform to penetrate the fluid in $\mathcal{V}$.

At two instances the flow map becomes degenerate.

i) As the blob sinks into $\mathcal{V}$, the boundary $\partial\mathcal{W}_t = \varphi_t(\partial\mathcal{W}_{t_0})$ becomes indefinitely stretched and since φ_t is assumed continuous on the entire fluid domain $\mathcal{D} = \bar{\mathcal{W}} \cup \bar{\mathcal{V}}$ (over-bar denotes closure), $\mathcal{V}$ cannot be severed by the motion of $\mathcal{W}$. A subset $\mathcal{S}$ gradually develops (dotted line in Figure 2b): this is where the inverse map φ_t^{-1} is multi-valued. The region $\mathcal{S}$, of 'virtual' separation, is mathematically interesting and physically important, but in most situations is ignored.

ii) As time passes the denser fluid gradually precipitates to the bottom surface of the box to reach equilibrium. As $t \to \infty$ the flow map φ_t becomes ill-defined for the points at the bottom surface of the box (Figure 2c).

Try this experiment with oil and vinegar.

Question 1.4 Does the topology of $\mathcal{V}$ change during the two stages of the process described in Example 1.3?

Problem 1.5 To classify degenerate flow patterns by using concepts from dynamical systems, graph theory and singularity theory.

For any fluid region $\mathcal{W}$ in $\mathcal{D}$ we have that

$$\partial \mathcal{W}_t = \varphi_t(\partial \mathcal{W}_{t_0}) \,, \tag{4}$$

which assures that any bounding fluid surface that is a material surface at time t_0, remains a material surface at all subsequent times t and moves with the flow (this follows from the definition of Φ). The *Jacobian* J of the transformation is defined by

$$J = \det\left(\frac{\partial x_i}{\partial a_j}\right) \,, \tag{5}$$

where the tensor $\partial x_i/\partial a_j$ represents the deformation of the infinitesimal volume as it is transported by the motion. The symmetric part of this tensor is associated with the distortion and change of the volume element, while the skew-symmetric part is associated with its rotation. From the assumption that φ possesses a differentiable inverse it follows that $0 < J < \infty$.

Vorticity is defined by $\boldsymbol{\omega} = \nabla \times \mathbf{u}$ and we assume that $\nabla \cdot \boldsymbol{\omega} = 0$ in $\mathcal{D}$. We have:

Definition 1.6 *The* **circulation** *(or* **flux of vorticity***) is defined by*

$$\kappa = \oint_{\mathcal{C}} \mathbf{u} \cdot d\mathbf{l} = \int_{\mathcal{S}} \boldsymbol{\omega} \cdot \hat{\boldsymbol{\nu}}\, d\sigma \,, \tag{5}$$

where $\mathcal{C}$ (of elementary directional length $d\mathbf{l}$) is a simple unknotted, closed circuit $\mathcal{C} \equiv \partial \mathcal{S}$, and $\mathcal{S}$ (of elementary area $d\sigma$) is a simply connected two-dimensional surface of unit normal $\hat{\boldsymbol{\nu}}$, pointing in the positive direction induced by the $\boldsymbol{\omega}$-field.

The two integrals are related by Stokes's theorem and in ideal conditions (Euler's equations) the common value $\kappa =$ constant is an *invariant* of fluid motion (Helmholtz's III law and Kelvin's theorem; see [30]). Moreover,

Definition 1.7 *The vorticity field $\boldsymbol{\omega}$ is said to be* **frozen** *in $\mathcal{D}$ if and only if it satisfies the transport (Helmholtz) equation*

$$\frac{\partial \boldsymbol{\omega}}{\partial t} = \nabla \times (\mathbf{u} \times \boldsymbol{\omega}) \,. \tag{6}$$

Exercise 1.8 Derive Helmholtz's equation from Euler's equations (2), assuming conservative body forces.

A formal solution to (6) is represented by the Cauchy equations

$$\omega_i(\mathbf{x}, t) = \omega_j(\mathbf{a}, t_0)\frac{\partial x_i}{\partial a_j} \,, \tag{7}$$

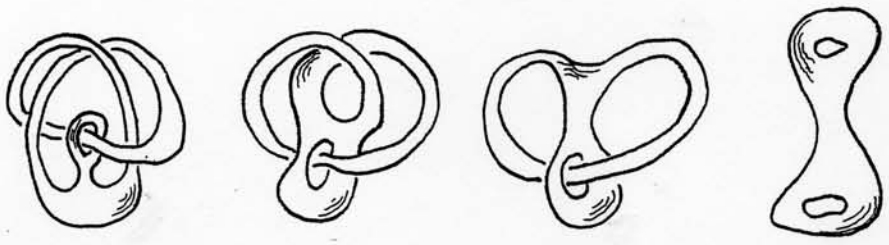

Figure 3. Topological equivalence between different configurations of the same fluid structure: (a) ~ (b) ~ (c) ~ (d).

that encapsulate both convection of the $\boldsymbol{\omega}$-field from $\mathbf{a}$ to $\mathbf{x}$, and rotation and distortion of the fluid elements by the deformation tensor $\partial x_i/\partial \mathrm{a}_j$ (incompressibility is given by the condition $\det(\partial x_i/\partial \mathrm{a}_j) = 1$). Since the tensor is a time-dependent diffeomorphism of position, it maps continuously (i.e. without cuts or reconnections) the initial field $\boldsymbol{\omega}(\mathbf{a}, t_0)$ to $\boldsymbol{\omega}(\mathbf{x}, t)$, thus establishing a *topological equivalence* between initial and final configuration (Figure 3). We write

$$\boldsymbol{\omega}(\mathbf{a}, t_0) \sim \boldsymbol{\omega}(\mathbf{x}, t)\,, \tag{8}$$

and we regard equation (6) as a master equation for frozen fields and equation (7) as a topological equivalence statement for the initial and final configuration fields.

For more information on general aspects of fluid mechanics a standard reference is [6]; on specific aspects of vortex dynamics a standard reference is [30].

2. Conserved Quantities in Ideal Fluids

In absence of dissipative and diffusive effects the invariance of circulation is of course just one manifestation of the ideal conditions of fluid motion. In this context it is natural to expect the existence of families of such quantities (not all necessarily scalars). One possible classification of invariants is based on their nature:

(*i*)	*local*	(*metric*)	$\longleftrightarrow$	*pointwise*
(*ii*)	*global*	(*metric*)	$\longleftrightarrow$	*integral*
(*iii*)	*topological*	(*non-metric*)	$\longleftrightarrow$	*algebraic*

As will be shown in §5 there are deep connections between continuum fluid mechanics and topology. To this regard a fundamental question is:

Problem 2.1 To classify and relate ideal fluid invariants and topological invariants.

Problem 2.1 finds a more natural setting in the language of differential forms. We shall briefly illustrate this point by showing how different conservation laws can be cast into one single differential form equation. We do this by concentrating the discussion on local invariants.

2.1. LOCAL INVARIANTS AND DIFFERENTIAL FORM CONSERVATION LAWS

Local fluid invariants can be classified in four categories:

I type: *conserved quantity* ρ (e.g. mass per unit volume).
Governing equation for scalar quantities as a balance conservation law:

$$\frac{\partial \rho}{\partial t} + \nabla \cdot (\rho \mathbf{u}) = 0 \, .$$

II type: *Lagrangian invariant* $\Im$ (e.g. a passive scalar, like ink).
Governing equation for scalar quantities advected Lagrangian invariantly by the flow:

$$\frac{d\Im}{dt} = \frac{\partial \Im}{\partial t} + (\mathbf{u} \cdot \nabla)\Im = 0 \, .$$

III type: *frozen-in vector field* $\boldsymbol{\omega}$ (e.g. vorticity).
Governing equation for vector quantities advected along the flow streamlines:

$$\frac{\partial \boldsymbol{\omega}}{\partial t} = \nabla \times (\mathbf{u} \times \boldsymbol{\omega}) \, .$$

IV type: *Frobenius invariant* $\mathbf{S}$ (e.g. momentum of a vortex ring).
Governing equation for vector quantities advected by Frobenius-type surfaces frozen in the flow (see Figure 4):

$$\frac{d\mathbf{S}}{dt} = (\mathbf{S} \times \nabla) \times \mathbf{u} \, .$$

All local fluid invariants can be classified in these four categories. These four types of invariants can be expressed in terms of differential forms, each one corresponding to an invariant ω^p-form ($p = 0, 1, 2, 3$) obeying the conservation law

$$\mathcal{L}_{t,\mathbf{u}} \omega^p \equiv \frac{\partial \omega^p}{\partial t} + \mathcal{L}_{\mathbf{u}} \omega^p = 0 \, . \tag{9}$$

Note that since $d\mathcal{L}_{\mathbf{u}} = \mathcal{L}_{\mathbf{u}} d$, equation (9) holds true also for $d\omega^p$, where $d\omega^p = \omega^{p+1}$; the four types of conservation laws are immediately recovered by setting $\omega^0 = \Im$, $\omega^1 = \mathbf{S}$, $\omega^2 = \boldsymbol{\omega}$ and $\omega^3 = \rho$.

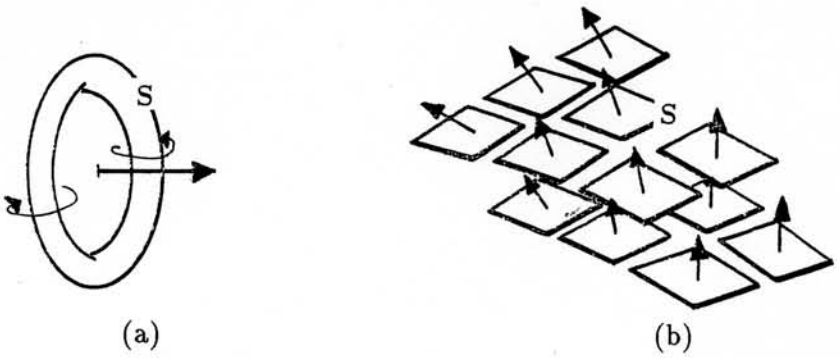

(a) (b)

Figure 4. (a) The toroidal surface of a vortex ring translating in an ideal fluid provides an example of a Frobenius surface for the linear momentum; (b) Frobenius surfaces frozen in the flow.

Exercise 2.2 Prove that the only non-vanishing differential forms in $\mathbb{R}^3$ are the ω^p-forms with $p = 0, 1, 2, 3$.

General relations between invariant p-forms and conservation laws can be derived from properties of differential forms [1, 10]. Similar considerations can be applied to global types of invariants. For an extensive study of these relations and possible connections with topological invariants see [34].

3. Geometric Dynamics of Vortex Filaments

Let us consider an isolated vortex filament (closed on itself or extending to infinity) in $\mathcal{D}$. We want to study the motion of the filament in terms of geometric quantities such as curvature and torsion and highlight aspects of motion that have interesting connections with integrable dynamics in soliton theory and problems in applied differential geometry of minimal surfaces. The analysis presented below has a long and fascinating history that goes back at least a hundred years (for more information see the review paper [26]).

3.1. INTRINSIC EQUATIONS OF MOTION IN EUCLIDEAN SPACE

To study the evolution of the filament in space we simply identify the filament with its vortex centreline Γ, smooth and free from inflections and self-intersections. The filament has, however, finite thickness and for simplicity we assume that its cross-section is circular, of radius $a \ll R$ (where R is the radius of curvature of Γ) and circulation κ. At an arbitrary point on Γ we position the origin of the intrinsic Frenet frame $(\hat{\mathbf{t}}, \hat{\mathbf{n}}, \hat{\mathbf{b}})$, unit tan-

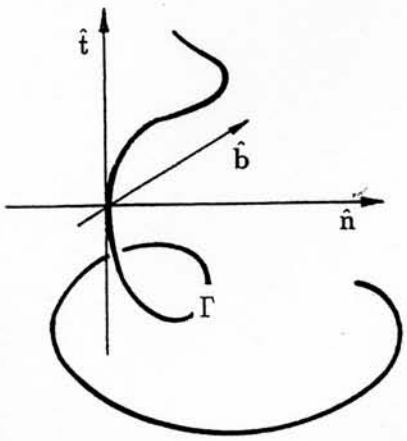

Figure 5. Intrinsic Frenet frame on a curve Γ.

gent, normal and binormal vectors to Γ (see Figure 5). Vorticity is simply given by $\boldsymbol{\omega} = \bar{\omega}\hat{\mathbf{t}}$, where $\bar{\omega}$ is a constant.

Remark 3.1 Given the distribution of vorticity $\boldsymbol{\omega}$, the standard problem is to find the induced velocity field $\mathbf{u}$ given by the Biot-Savart integral [30].

Let $\mathbf{X} = \mathbf{X}(s,t)$ (s arc-length) denote the vortex line Γ and $\hat{\mathbf{t}} \equiv \mathbf{X}'$ (prime denotes arc-length derivative). Tangent, normal and binormal are well-defined everywhere on the curve and satisfy the *Serret-Frenet equations*

$$\hat{\mathbf{t}}' = c\hat{\mathbf{n}} \ , \quad \hat{\mathbf{n}}' = -c\hat{\mathbf{t}} + \tau\hat{\mathbf{b}} \ , \quad \hat{\mathbf{b}}' = -\tau\hat{\mathbf{n}} \ , \tag{10}$$

where τ is torsion. Let $\mathbf{v} \equiv \dot{\mathbf{X}}$ be the velocity induced by vorticity; in intrinsic components we have $\mathbf{v} = (v_t, v_n, v_b)$, where everything is a smooth function of s and t (over-dot denotes time derivative). Since $\dot{\hat{\mathbf{t}}} = \dot{\mathbf{X}}' = \mathbf{v}'$, after some algebra we can derive the intrinsic equations of motion of the vortex filament in $\mathcal{D}$. Assuming (for simplicity) inextensibility of Γ we have *two intrinsic equations*

$$\dot{c} = (cv_t + v_n' - \tau v_b)' - (\tau v_n + v_b')\tau \ , \tag{11}$$

$$\dot{\tau} = \left[\frac{(cv_t + v_n' - \tau v_b)\tau + (\tau v_n + v_b')'}{c}\right]' + (\tau v_n + v_b')c \ . \tag{12}$$

that give the time-evolution of curvature and torsion of the filament in terms of the initial geometry and induced velocity. The condition of inextensibility is satisfied when the curve is parametrized by arc-length; this condition is expressed by the third equation (*congruence condition*)

$$v_t' = cv_n \ . \tag{13}$$

A full derivation of equations (11)–(13) can be found in [26].

Exercise 3.2 (i) Prove the validity of condition (13) for arc-parametrized curves. (ii) Using eqs. (11)–(12) study the case of a circle that shrinks with a velocity proportional to the curvature.

Exercise 3.3 Suppose $\mathbf{v} = v_b(c,\tau)\hat{\mathbf{b}}$ where v_b is a smooth function of c and τ. Prove that in the stationary case (i.e. with $\dot{c} = 0$ and $\dot{\tau} = 0$) eqs. (11-12) admit two integrals of motions given by:

$$W_1 = v_b^2\tau = \text{constant} , \tag{14}$$

and

$$W_2 = \frac{v_b'' - v_b\tau^2}{c} + v_b c - \int_\Gamma v_b c'\, ds = \text{constant} . \tag{15}$$

3.2. INTEGRABILITY AND GLOBAL GEOMETRIC INVARIANTS

In the previous section we didn't specify the induced velocity $\mathbf{v}$ of the filament. In actual fact this velocity is determined by the prescribed vorticity by 'un-curling' (through the Biot-Savart integral) the equation $\boldsymbol{\omega} = \nabla \times \mathbf{v}$. Given the vorticity (i.e. its distribution over the cross-section) we thus obtain specific functional relationships for v_t, v_n and v_b. We have further (analytical) difficulties when we consider more realistic vortex motions, for instance in presence of a varying cross-section and vorticity distribution). The simplest case of a vortex line with $\boldsymbol{\omega} = \bar{\omega}\hat{\mathbf{t}}$ (see §3.1) reveals interesting connections with integrable systems. The asymptotic theory developed for this case [26] shows that the motion, goverened by the so-called *localized induction approximation* (LIA), is given (after appropriate re-scaling) by:

$$\text{LIA}: \qquad v_t = 0 , \quad v_n = 0 , \quad v_b = c . \tag{16}$$

Under LIA the intrinsic equations (11)–(12) take a much simpler form known as *Da Rios–Betchov equations.*

Exercise 3.4 Under LIA reduce eqs. (11)–(12) to the Da Rios–Betchov equations and directly from these latter find the two integrals of motion, particular cases of W_1 and W_2 of Exercise 3.3.

By applying a Madelung transformation in the form

$$\psi(s,t) = c(s,t)\, e^{i\int_\Gamma \tau(\bar{s},t)\, d\bar{s}} , \qquad \psi(s,t) \in \mathbb{C}^1 , \tag{17}$$

we can map points from the (c, τ)-space to the complex plane in $\mathbb{C}^1$, thus reducing the two intrinsic equations (11)–(12) in c and τ to one single equation in ψ. By using eq. (17) Hasimoto [12] finds a remarkable relationship between LIA and the *non-linear Schrödinger equation* (NLSE)

$$\frac{1}{i}\frac{\partial \psi}{\partial t} = \frac{\partial^2 \psi}{\partial s^2} + \frac{1}{2}|\psi|^2 \psi \,, \tag{18}$$

that in one dimension admits solutions in terms of solitary waves (*solitons*). From soliton theory we know that NLSE is indeed completely integrable and has an infinite (countable) number of *conservation laws* in involution. Under LIA vortex filament motion and integrable dynamics of soliton theory are thus related so that we can interpret mathematical aspects of soliton systems in terms of fluid dynamical properties. One interesting aspect regards the existence of soliton invariants. Since ψ is a well-defined one-to-one mapping from the solution space in (c, τ) to the complex plane, its inverse is also well-defined. By applying the inverse map ψ^{-1} we can express the family of conservation laws, obtained directly from (18), in terms of global geometric functionals; the first three of them (neglecting the constant quantities) are

$$\int_\Gamma c^2 \, ds \,, \quad \int_\Gamma c^2 \tau \, ds \,, \quad \int_\Gamma \left(\frac{c^4}{4} - c'^2 - c^2 \tau^2 \right) ds \,, \quad \ldots \,, \tag{19}$$

where these integrals are all constants of the motion (invariant in time). The set, however, is not complete and other integral quantities, not captured by the NLSE theory, are also conserved. Few of these quantities admit physical interpretation in terms of kinetic energy, helicity, linear and angular momenta of the vortex filament (all conserved quantities under LIA as well as under Euler's equations), whereas the remaining provide a purely geometric information (including total torsion, writhing, etc.) [24].

In recent years more work has been dedicated to extend these connections between vortex motion and integrability. As Fukumoto & Miyazaki show [11], in presence of axial flow vortex filament motion can be reduced to a Korteweg-de Vries type of equation, another soliton equation with infinite number of conservation laws in involution. Further generalizations (to include Hirota type equations and sine-Gordon equations) are also possible. How general can we go to preserve integrability on one hand and vortex motion on the other? And, is this a route towards integrability of Euler's equations? Asymptotic analyses based on Biot-Savart integral reveal an increasing analytical complexity and it is doubtful that additional information (given, for example, by tube thickness and distribution of vorticity) can preserve integrability. Work in this direction is carried out, among oth-

ers, by Fukumoto and collaborators. An interesting open question seems to be the following:

Problem 3.5 To determine under which general geometric conditions the motion of a vortex line is completely integrable.

Langer & Perline [17] discovered interesting geometric relationship (not necessarily satisfying the laws of vortex motion) between LIA-type of equations and the hierarchy of integrable one-dimensional systems. Their approach, based on the study of the Hamiltonian structure associated with a class of soliton equations and their Poisson geometry, shows that it is possible to define a recursive operator $\Re$, that, starting from LIA, generates integrable dynamics in cascade. The operator can be explicited as

$$\Re: \quad \begin{cases} \dot{\mathbf{X}}^{(0)} = c\hat{\mathbf{b}} \,, \\ \dot{\mathbf{X}}^{(j)} = \hat{\mathbf{t}}^{(j-1)} \times \hat{\mathbf{t}} + \left[\int c(\bar{s},t)(v_b'^{(j-1)} + \tau v_n^{(j-1)})d\bar{s}\right]\hat{\mathbf{t}} \,, \end{cases} \tag{20}$$

where $j = 1, 2, \ldots$. Note that the recursive operator (20) preserves arc-length parametrization. General conditions for integrability of space curves and relations to Bäcklund transformations and Lax pairs can be found in [22].

Finally, since the motion of Γ is governed by the principle of least action, the surface (in s and t) swept out by Γ during the motion is a minimal surface for kinetic energy. In the case of integrable dynamics, we may have a natural connection between soliton theory and Plateau problems, and more precisely between characteristic properties of soliton surfaces and geometric aspects of minimal surfaces in the metric given by the kinetic energy of the system. The situation is illustrated by the graph below:

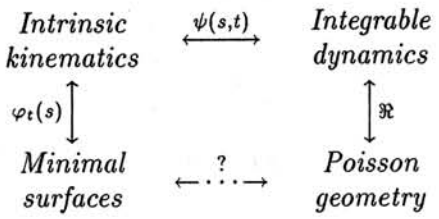

3.3. EXTENSION TO HIGHER DIMENSIONAL MANIFOLDS

The intrinsic equations (11)–(13) can be extended to $2n+1$-dimensional manifolds $\mathcal{M} \cong \mathbb{R}^{2n+1}$, where Γ is now an arc-parametrized curve in $\mathcal{M}$. The $(0,2)$-type *metric tensor* g is a smooth and positive-definite section of the bundle of the symmetric bi-linear two-forms on $\mathcal{M}$, given by $g =$

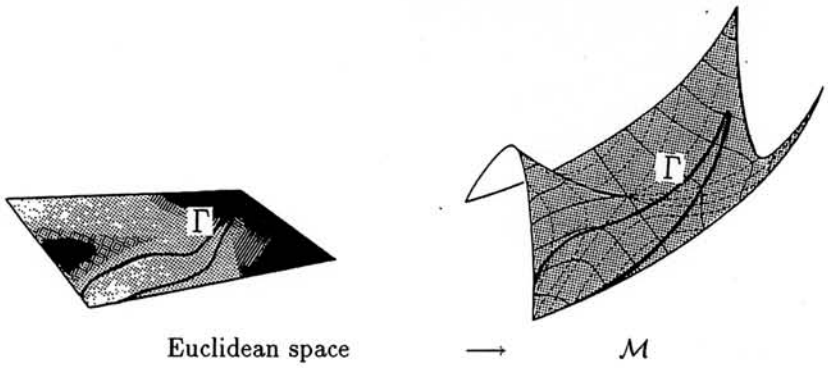

Figure 6. Geometrization of compressibility in the Euclidean space by the curvature tensor of $\mathcal{M}$.

$g_{ij}\,dx^i \otimes dx^j$. Given a C^r linear connection ∇ on $\mathcal{M}$, one can define a C^{r-1} *torsion tensor* T of type $(1,2)$ by

$$\mathsf{T}(\mathsf{Y},\mathsf{Z}) = \frac{1}{2}\left(\nabla_{\mathsf{Y}}\mathsf{Z} - \nabla_{\mathsf{Z}}\mathsf{Y} - [\mathsf{Y},\mathsf{Z}]\right) ,$$

and a C^{r-1} *Riemann (curvature) tensor* R of type $(3,1)$ by

$$\mathsf{R}(\mathsf{Y},\mathsf{Z})(\mathsf{V},\mathsf{W}) = \left[\nabla_{\mathsf{Y}}\nabla_{\mathsf{Z}}g(\mathsf{W}) - \nabla_{\mathsf{Z}}\nabla_{\mathsf{Y}}g(\mathsf{W}) - \nabla_{[\mathsf{Y},\mathsf{Z}]}g(\mathsf{W})\right](\mathsf{V}) ,$$

where $[\mathsf{Y},\mathsf{Z}]$ is the Lie derivative of Z with respect to Y and $\mathsf{V},\mathsf{W},\mathsf{Y},\mathsf{Z}$ are arbitrary C^{r+1} fields.

The Serret-Frenet equations (10) take the general form given by the $SO(2n+1)$-structure for the generalized $2n$ curvatures $\Omega_i^j = -\Omega_j^i$ $(i,j = 1,\ldots,2n+1)$, where Ω_i^j are sufficiently smooth functions of s and t. The generalized induced velocity has components v^j in the basis $\{e_j\}$ given by the metric g. By applying Ricci formula, and after some tedious but straightforward algebra, we obtain the *intrinsic equations in generalized form* [23]:

$$v^1{}_{,s} = 2\mathsf{T}^t_{st}v^1 - \Omega^1_2 v^2 + 2\mathsf{T}^s_{st} \qquad \text{for} \quad k = 1 , \tag{21}$$

$$\dot{\Omega}^k_{k-1} = A^k_k - \Omega^k_{k-1}\left(\sum_{i=1}^{k-2}\frac{\dot{\Omega}^{i+1}_i}{\Omega^{i+1}_i} - 2k\mathsf{T}^s_{st}\right) , \tag{22}$$

where

$$A^k_1 = v^k_{,s} + v^{\bar{k}}\Omega^k_{\bar{k}} - 2\mathsf{T}^t_{st}v^k ,$$

$$A^k_k = A^k_{(k-1),s} + A^{\bar{k}}_{k-1}\Omega^k_{\bar{k}} - 2\mathsf{T}^t_{st}A^k_{k-1} - \Omega^{k-2}_{k-1}A^k_{k-2} ,$$

for $k = 2, \ldots, 2n+1$, and $\bar{k} = k-1, k+1$. Equation (21) represents the congruence condition for the arc-parametrized curve Γ and (22) gives $2n$ intrinsic equations for the time evolution of the curvatures Ω_j^i in $\mathcal{M}$.

Remark 3.6 By taking g, T and R pointwise functions of density (via the Jacobian J) we can geometrize the compressibility of the ambient space by prescribing appropriate functional relationships between the connection coefficients (hence the components of the torsion and curvature tensors) and J (see Figure 6). In this way extension to higher dimensional manifolds provides a route to a geometrization of fluid mechanical properties.

More information on geometric properties of fluid flows can be found in the seminal papers by Arnold [3] and Ebin & Marsden [9], and in more recent works by Holm, Marsden & Ratiu [13] and Shkoller [32].

4. Vortex Knots and Links and Reidemeister's Moves

Vortex flux tubes are coherent bundles of vortex lines embedded in a tube-like region. If the tube axis (which is a vortex line) is in the shape of a knot or a link, the corresponding vortex flux tube, formed by the tubular neighbourhood of vortex lines, is also knotted or linked. Formally, knotted and linked flux tubes can be constructed in a standard way as indicated, for example, by Moffatt [19] (see also [20]), that is via standard embedding, Dehn's surgery and appropriate cross-switchings. A formal definition of knotted or linked vortex tubes is given here. Let us consider first the following:

Definition 4.1 *A surface $\mathcal{S}$ is a* **vortex surface** *in $\mathcal{D}$ if it is made of vortex lines that are everywhere tangent to this surface.*

As we remarked in §1 an ideal vortex surface $\mathcal{S}$ at time $t = t_0$ remains a vortex surface $\mathcal{S}_t$ at every subsequent time, since $\mathcal{S}_t = \varphi_t(\mathcal{S}_{t_0})$.

Consider the standard solid torus T in $\mathbb{R}^3$ given by

$$((2 + \epsilon\cos\beta)\cos\alpha,\ (2 + \epsilon\cos\beta)\sin\alpha,\ \epsilon\sin\beta)\ , \tag{23}$$

where $\alpha \in [0, 2\pi]$, $\beta \in [0, 2\pi]$ and $\epsilon \in [0, 1]$. Let $\mathcal{F}_{p,q}$ ($p > q > 1$ co-prime integers) denote the foliation of T by the curves $\Gamma_{\epsilon,\beta}$ given by

$$\Gamma_{\epsilon,\beta}(s) = \left\{ \begin{array}{c} [2 + \epsilon\cos(\beta + qs)]\cos(ps) \\ [2 + \epsilon\cos(\beta + qs)]\sin(ps) \\ \epsilon\sin(\beta + qs) \end{array} \right\}\ , \tag{24}$$

where $s \in [0, 2\pi]$. We have

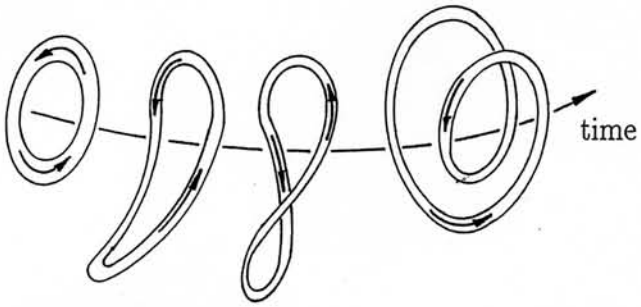

Figure 7. Stretching of a vortex filament is produced by tangential actions on the tube strands. This deformation leaves the filament in the same topological class.

Definition 4.2 *A collection of* **linked (knotted) vortex tubes** $\mathcal{L}_v$ *is defined as a smooth embedding in* $\mathcal{D}$ *of finitely many disjoint standard solid tori* $\sqcup_i T_i$, *and smooth vorticity* $\boldsymbol{\omega}$ *such that:*

(i) $\mathcal{L}_v$ *is an embedding when restricted to the interior of* $\sqcup_i T_i$;

(ii) the bounding surface $\mathcal{S} \equiv \sqcup_i \mathcal{L}_v(\partial T_i)$ *is a vortex surface;*

(iii) for each component $\mathcal{L}_v(T_i)$ *there exists a pair* $\{p_i, q_i\}$ *(*$p_i > q_i > 1$ *co-prime integers) such that* $\mathcal{L}_v$ *maps the foliation* $\mathcal{F}_{p_i,q_i}$ *of* T_i *onto the integral curves of* $\boldsymbol{\omega}$ *in* $\mathcal{L}_v(T_i)$.

If p and q are real numbers, p/q is irrational and we can extend the definition to vortex tubes formed by non-closed vortex lines (of support $\Gamma_{\epsilon,\beta}$) space-filling the tori $\sqcup_i T_i$.

Since vorticity is frozen in $\mathcal{D}$, linked (knotted) vortex filaments are also frozen in their topological equivalence class. Topological fluid mechanics deals essentially with the study of fluid structures (thought of as embeddings) that can be continuously deformed one into another by ambient isotopies. For example, a natural isotopic deformation is represented by stretching of vortex tubes (geometrically equivalent to a time-dependent re-parametrization of the tube centreline, see Figure 7).

From knot theory we know that topology is preserved under the action of Reidemeister's moves. In the context of the Euler equations these moves are performed quite naturally by the action of local flows on the strands of fluid structures. If the background fluid in the complement $(\mathcal{D} - \mathcal{L}_v)$ is irrotational and at rest, then these flows must satisfy the Dirichlet problem for the Laplacian of the stream function ψ, given by

$$\begin{cases} \mathbf{u} = \nabla\psi \\ \nabla^2\psi = 0 \end{cases} \qquad \text{in} \quad (\mathcal{D} - \mathcal{L}_v)\,, \tag{25}$$

with boundary conditions

$$\begin{aligned} &\mathbf{u}\cdot\hat{\boldsymbol{\nu}} = u_\perp \qquad \text{on} \quad \mathcal{S} \equiv \sqcup_i \mathcal{L}_v(\partial T_i)\ , \\ &\mathbf{u} = 0 \qquad\quad\ \ \text{as} \quad \mathbf{x}\to\infty\ , \end{aligned} \tag{26}$$

where $u_\perp = u_\perp(\mathbf{x},t)$ is the normal component of the velocity on the vortex boundary surface, with $\hat{\boldsymbol{\nu}}$ denoting the normal vector to the surface. Equations (25) and (26) have a unique solution in terms of local flows [6]. These flows act by performing a sequence of Reidemeister's moves on the tube strands through continuous deformations. Note that the boundary condition (26) does not prescribe the tangential component of the velocity on the bounding vortex surface. As we pointed out earlier, tangential effects (present for instance if the tube gets stretched) preserve vortex topology. This means that Reidemeister's moves are performed by local flows that are solutions to (25–26), up to arbitrary tangential actions.

For some historical information and a simple introduction to topological fluid mechanics see the review article by Ricca & Berger [28].

5. Helicity and Linking Numbers

A fundamental question in topological fluid mechanics is to understand whether and how fluid and topological invariants relate one another. A fundamental result regards kinetic helicity and its topological interpretation.

Definition 5.1 *The* **kinetic helicity** *of a linked (knotted) vortex system $\mathcal{L}_v$ in $\mathcal{D}$ is defined by*

$$H(\mathcal{L}_v) = \int_{\sqcup_i \mathcal{L}_v(T_i)} \mathbf{u}\cdot\boldsymbol{\omega}\, d^3\mathbf{x}\ . \tag{27}$$

Helicity is the fluid dynamical version of the Hopf integral, i.e. the integral of the inner product of a solenoidal vector field and its curl; isotopy invariance of this quantity was discovered by Whitehead in 1947. However, in the context of ideal fluid mechanics conservation of helicity (kinetic and magnetic) was shown by the works of Woltjer (1958), Moreau (1961), Moffatt (1969) and Arnold (1974) (see [18, 4]).

A fundamental result that establishes a bridge between topology and fluid mechanics regards the topological interpretation of helicity in terms of linking numbers. We have:

Theorem 5.2 ([18, 8, 20]) *Let $\mathcal{L}_v$ be a collection of vortex links (knots). Then*

$$H(\mathcal{L}_v) = \sum_i Lk_i\,\kappa_i^2 + 2\sum_{i\neq j} Lk_{ij}\,\kappa_i\kappa_j\ , \tag{28}$$

where Lk_i denotes the (Călugăreanu-White) linking number of the tube axis of $\mathcal{L}_v(T_i)$ with respect to the framing induced by the embedding of the ω-field, and Lk_{ij} denotes the (Gauss) linking number of $\mathcal{L}_v(T_i)$ with $\mathcal{L}_v(T_j)$.

Let $\mathcal{L}_v(T) \equiv \mathcal{K}_v(T)$ be a single vortex knot. Then, equation (28) reduces to

$$H(\mathcal{K}_v) = Lk\,\kappa^2 = (Wr + Tw)\,\kappa^2 \,, \tag{29}$$

where we write the (Călugăreanu-White) linking number Lk in terms of its decomposition given by the writhing number Wr of the tube axis and total twist Tw of the vortex tube (for a precise definition of these quantities see the article of Langevin, this volume, and Moffatt & Ricca [20]). Note that writhe and twist are purely geometric quantities and their values change with a change of shape. This means that Wr and Tw change continuously under continuous deformation, their sum remaining constant in time.

The writhing number Wr is characterized by the following properties:

i) Wr depends only on the geometry of the tube axis;

ii) Wr is invariant under rigid motions or dilations of the ambient space (conformal invariant), but its sign changes under reflection;

iii) in passing from an under-crossing to an over-crossing of the tube strands (in a given projection plane), its value jumps by $+2$.

Exercise 5.3 Show that the writhing number of a curve Γ (as defined by the integral formula given in Langevin's article, this volume) admits physical interpretation in terms of the sum of the signed crossings of the diagram of Γ in a given projection plane, averaged over all projections, that is

$$Wr = < n_+(\hat{\boldsymbol{\nu}}) - n_-(\hat{\boldsymbol{\nu}}) > \,, \tag{30}$$

where the angular brackets denote averaging over all directions $\hat{\boldsymbol{\nu}}$ of projection, and $n_\pm$ denotes the number of apparent $\pm$ crossings, from the direction of projection $\hat{\boldsymbol{\nu}}$. Derive eq. (30) directly from the integral formula.

Remark 5.4 For a nearly plane curve (except small indentations to allow crossings) the writhe of the curve can be estimated by counting the sum of the signed crossings that are apparent from that plane projection (see Figure 8).

The normalized total twist Tw is given by the sum of the total torsion of the tube axis and the intrinsic twist of the ω-lines in the tube T, divided by 2π, and has the following properties:

i) Tw is a continuous function of the tube axis;

ii) Tw is invariant under rigid motions or dilations of the ambient space (conformal invariant), but changes sign under reflection;

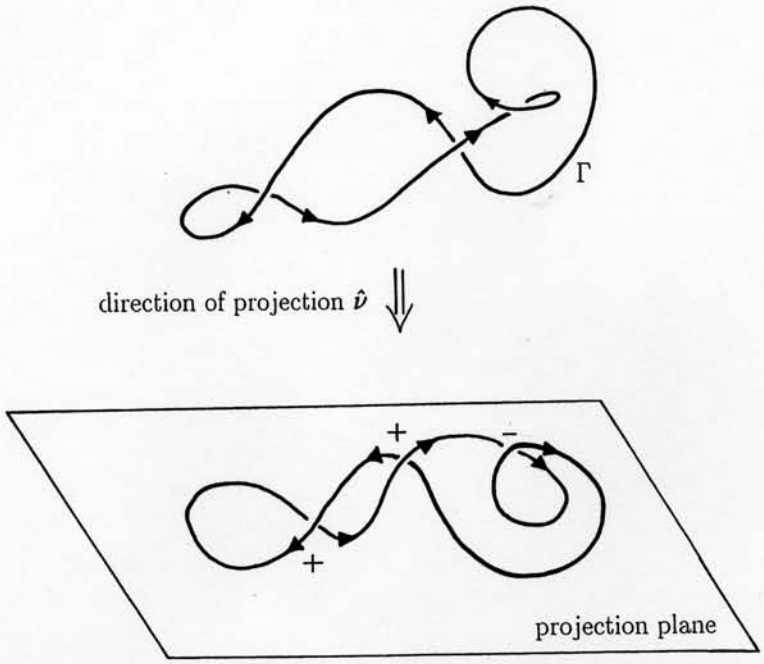

Figure 8. The writhing number of an oriented curve can be estimated by counting the sum of the signed crossings of the diagram of the curve projected on the plane along the direction $\hat{\nu}$, then averaging over all directions.

iii) Tw is additive for contiguous tubular segments of T.

Part of the twist contribution to helicity is therefore associated with torsion of the tube axis and part with what may be described as 'intrinsic twist' of the field lines in the vortex flux tube.

If the embedding of the ω-lines corresponds to a zero-framing of each component $\mathcal{L}_v(T_i)$ (i.e. $Lk_i = 0$ for each i-th component), then

$$H(\mathcal{L}_v) = 2 \sum_{i,j} Lk_{ij}\, \kappa_i \kappa_j \ . \tag{22}$$

Note that as shown in Figure 9 there are cases of non-trivial zero-framed vortex links with zero (Gauss) linking number Lk_{ij} and thus zero total helicity.

Higher-order linking numbers able to classify topologies otherwise not captured by the standard Gauss linking number (as in the case of the Borromean rings) have been studied by Berger [7]. Since links are close relatives of braids, a hierarchy of linking integrals generates a family of winding numbers for braids. Higher-order helicity integrals for braided fluid structures are based on these invariants.

Figure 9. The Borromean configuration for three zero-framed linked vortex tubes provides an example of zero (Gauss) linking number: the total helicity of this system is zero!

For more information on aspects of helicity and fluid flows see the review article by Moffatt and Tsinober [21] and the book by Arnold and Khesin [4].

6. Evolution of Vortex Knots and Links

6.1. THIN CORED VORTEX KNOTS

Thin vortex knots have been found as solutions to the localized induction approximation (LIA; see §3.2). Remember that this is an approximation of the Biot-Savart law of Euler's equations. Existence and steadiness of knotted solutions to LIA have been studied by Kida [15] and Keener [14]. Kida's solutions are torus knots in the physical space. We have:

Theorem 6.1 ([15]) *Let $\mathcal{K}_v$ denote the embedding of a knotted vortex filament in an ideal fluid in $\mathcal{D}$. If $\mathcal{K}_v$ evolves under LIA, then there exists a class of steady solutions in the shape of torus knots $\mathcal{K}_v \equiv \mathcal{T}_{p,q}$.*

In geometric terms Kida's solutions are closed curves embedded on a mathematical torus Π, wrapping the torus $p > 1$ times in the longitudinal direction and $q > 1$ times in the meridian direction (p, q co-prime integers). The winding number is given by $w = q/p$, and self-linking given by $Lk = pq$, two topological invariants of the knot type. Kida finds torus knot solutions in terms of fully non-linear relationships that involve elliptic functions of traveling waves.

Torus knots have two isotopes $\mathcal{T}_{p,q}$ and $\mathcal{T}_{q,p}$ (for given p and q), that are topologically equivalent but geometrically different. Since vortex filament motion is influenced by the curve geometry (and in particular by curvature), the question of evolution and stability of the two isotopes is particularly interesting. By using linear perturbation techniques and cylindrical polar coordinates (r, α, z) it is possible to obtain 'small-amplitude' torus knot solutions that are asymptotically equivalent to those of Kida.

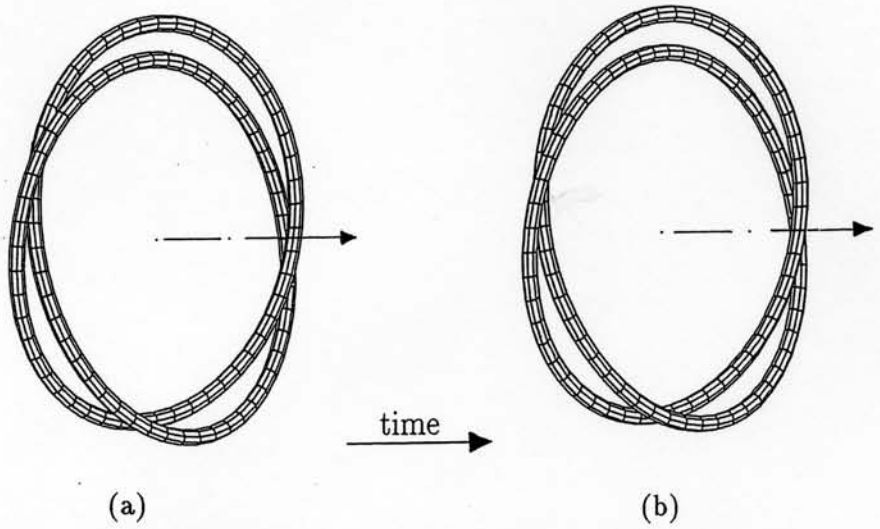

Figure 10. Evolution of torus knot $\mathcal{T}_{2,3}$ under LIA. (a) Initial configuration; (b) configuration at a later time. The knot evolution is stable as predicted by the LIA analysis. The tube shown is merely an aid to visualize vortex evolution [28].

The advantage of this approach is that we can write the solutions in terms of simple trigonometric functions amenable to further analysis. A linear stability analysis based on this approach gives the following result:

Theorem 6.2 ([25]) *Let $\mathcal{T}_{p,q}$ denote the embedding of a 'small-amplitude' vortex torus knot $\mathcal{K}_v$ evolving under LIA. $\mathcal{T}_{p,q}$ is steady and stable under linear perturbations iff $q > p$ $(w > 1)$.*

Numerical simulations have been carried out to check and investigate properties of torus knot evolution based on the result of Theorem 6.2 [29]. Under LIA torus knots with winding number $w > 1$ translate and rotate uniformly and steadily in space as rigid bodies. In the case of $w < 1$, however, instabilities develop almost immediately and the knot unfolds towards reconnection events.

Figure 10 shows two snapshots of the stable knot $\mathcal{T}_{2,3}$ and Figure 11 shows the knot $\mathcal{T}_{3,2}$ when it becomes unstable and unfolds. These simulations led to the discovery of a strong stabilizing effect present when the full Biot-Savart law governs the evolution of LIA unstable knots. This is a rather intriguing effect that merits further investigation. A beautiful applied mathematics problem is:

Problem 6.3 Given a vortex filament in the shape of a torus knot $\mathcal{T}_{p,q}$, with circular cross-section and uniform distribution of vorticity, to find the induced velocity in terms of analytical solution of the Biot-Savart integral.

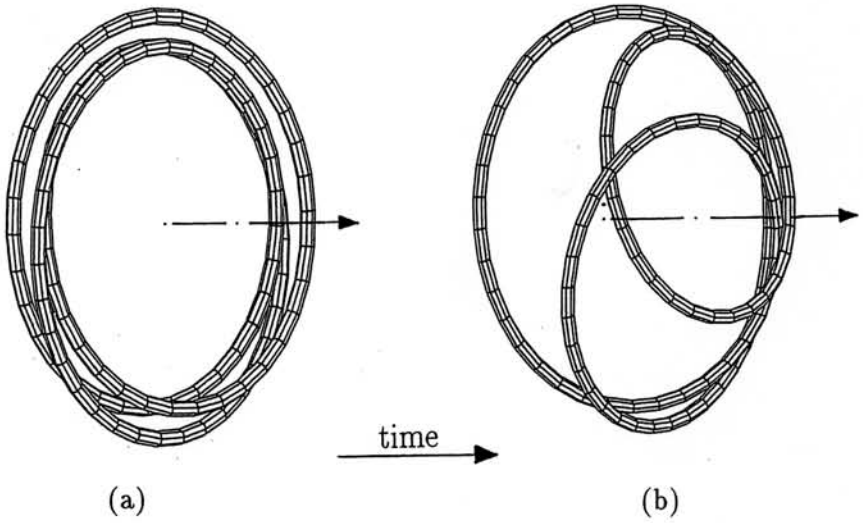

Figure 11. Evolution of torus knot $\mathcal{T}_{3,2}$ under LIA. (a) Initial configuration; (b) configuration at a later time. The knot evolution is unstable according to the LIA analysis and unfolds immediately [28].

Another interesting aspect of current research is represented by possible links between soliton invariants and torus knot solutions. Since LIA and NLSE are related via the Hasimoto map (17), the infinite number of conserved quantities in involution expressed in terms of global geometric functionals (19) are also constants of motion of Kida's torus knot solutions. Finding connections between this family of invariants and the polynomial invariants of knots could represent an important step towards closer links between differential geometry, geometric topology and integrability theory.

6.2. THIN CORED VORTEX LINKS

From a mathematical viewpoint little work is done on vortex links, the only known results being those of J.J. Thomson [33] more than a century ago. Thomson considers particularly symmetric systems of links that travel in steady motion as rigid bodies in the fluid. The simplest case is represented by the Hopf link obtained by embedding two vortex rings Γ_1 and Γ_2 equally spaced on the surface of a mathematical torus Π of radius R and small diameter d. This link system can be realized by the following 'thought construction': choose a meridian plane of Π and place two point vortices (representing the cross-sections of the vortex filaments) on the circumference in diametrically opposite position. Consider now the simultaneous uniform rotation of the two point vortices around the common

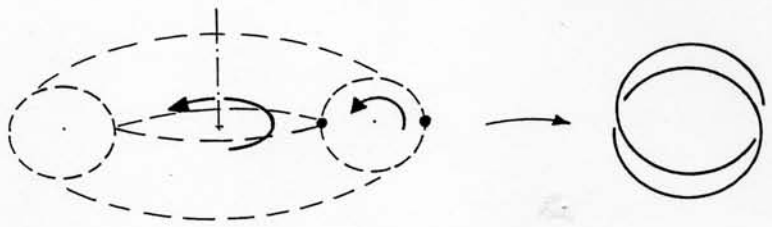

Figure 12. Interpretation of J.J. Thomson's 'thought construction' of a Hopf vortex link system ($n = 2$, $Lk = 1$).

center of mass (i.e. the center of the meridional circumference) *and* around the principal axis of the torus, along the great circle of radius R, in the longitudinal direction (see Figure 12). The vortex link system results from the collection of the two point vortex positions occupied after their full (double) revolution.

Let $\lambda = \max|\mathbf{X}_i - \mathbf{X}_i^*|$, for points $\{\mathbf{X}_i, \mathbf{X}_i^*\} \in \Gamma_i$, $i = 1, 2$, and $\delta = \min|\mathbf{X}_1 - \mathbf{X}_2|$ for points $\mathbf{X}_1 \in \Gamma_1$ and $\mathbf{X}_2 \in \Gamma_2$. Assuming that $\lambda \gg \delta$, where $\lambda = O(R)$ and $\delta = O(d)$, we have:

Theorem 6.4 ([33]) *Consider the Hopf link given by two vortex rings of equal circulation κ and relative linking number Lk, embedded and equally spaced on a torus Π in $\mathcal{D}$. The vortex system is steady and stable iff*

$$\frac{M(2\pi\rho\kappa)^{1/2}}{LkP^{3/2}} < 1\,, \tag{31}$$

where ρ is the fluid density (constant) and $M = |\mathbf{M}|$ and $P = |\mathbf{P}|$ are the intensities of the angular momentum $\mathbf{M}$, and the linear momentum $\mathbf{P}$ of the system.

This is a remarkable result that combines geometry, topology and fluid dynamics. The simplest link system (with $Lk = 1$) rotates and translates with angular velocity Ω and translational velocity V given by

$$\Omega = \frac{\kappa}{\pi d^2}\,, \quad V = \frac{\kappa}{4\pi R}\log\frac{64R^2}{a^2}\,. \tag{32}$$

Higher-order two-component link systems (i.e. with $Lk > 1$) are obtained by increasing the number of full revolutions of the point vortex system around the great circle (see Figure 13a).

Consider now n vortex rings linked together. As above, the system can be thought of as generated by full revolutions of n point vortices (equally spaced on the small circumference) around the two principal axes of Π (in the longitudinal and meridian direction) to obtain n-vortex components linked in space (see Figure 13b). We have

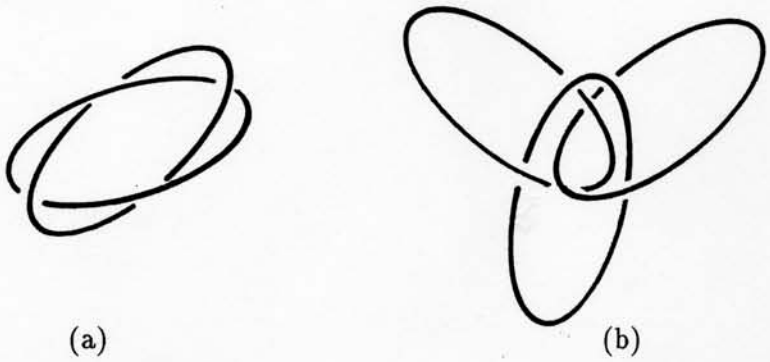

Figure 13. (a) A higher-order Hopf link with $n = 2$, $Lk = 2$; (b) a link of $n = 3$ components with relative linking $Lk = 1$.

Theorem 6.5 ([33]) *Consider the link of n vortex rings of equal circulation κ and relative linking number Lk, embedded and equally spaced on a torus Π in $\mathcal{D}$. The vortex system is steady and stable iff $n \leq 6$.*

This result, applied to a system of n point vortices in the plane, has been refined by other authors (for more information see [30]). For recent numerical works on simulations of vortex link production see [2] and for reconnection and dissipation of a trefoil vortex knot see [16].

7. Algebraic, Geometric and Topological Measures of Flow Complexity

Measuring structural complexity in vortex flows is becoming an important aspect of fluid mechanics research. On one hand progress in geometric and topological fluid mechanics and dynamical system theory give new tools to explore dynamical aspects of fluid flows, including knotting and linking of flow patterns, on the other hand numerical and computational progress make now possible analyses and visualizations (visiometrics) of mechanisms (such as vortex reconnection) with unprecedented details. Many mathematical concepts already developed are available for numerical implementation and new ones are being put forward for application on test cases.

Based on the idea of a *tropicity domain*, given by the 'numerical' domain determined by a computed vortex tangle (see, for example, Figure 14), we can determine principal directional axes (*tropicity axes*) to measure degrees of *tubeness*, *sheetness* and *bulkiness* of the vortex system and relative spread of flow lines (particle paths, streamlines, vortex lines) [27].

For discrete vortex tangles (produced numerically by a simulation or naturally in superfluids) *directional writhing* $Wr(\hat{\boldsymbol{\nu}})$ provides an estimate of the geometric average coiling of projected vortex lines. This measure is

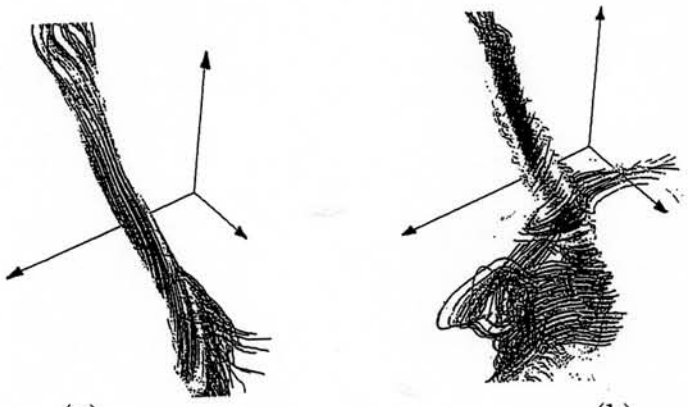

Figure 14. (a) Computed vortex lines and (b) streamlines of a vortex tube produced by direct numerical simulation of homogeneous, isotropic turbulence [30].

simply given by the writhing number Wr of the oriented graph resulting from the projection of the tangle onto a projection plane of normal $\hat{\boldsymbol{\nu}}$. By keeping track of the orientation of the curve (induced by vorticity) and by assigning the value $\epsilon_r = \pm 1$ to each projected crossing r (according to the standard convention on crossing signs; cf. eq. 30 of §5), we can calculate the directional writhing by

$$Wr(\hat{\boldsymbol{\nu}}) = \sum_r \epsilon_r \ , \qquad Wr = <\sum_r \epsilon_r>_{\mathcal{D}} \ , \tag{33}$$

whereas the writhing number Wr is given by averaging the directional writhe over the whole domain. We can show [5] that this quantity is well aproximated by the *estimated writhing*

$$Wr_{\perp} = <\sum_r \epsilon_r>_{\perp} \approx Wr \ , \tag{34}$$

obtained by taking the algebraic mean over the three principal orthogonal planes ($x = y = z = 0$), that gives a simple, direct measure of the average coiling of the tangle in space.

Structural complexity is also measured by counting the total number of apparent crossings present at a given time. This quantity, which is associated with un-oriented tangle diagrams, is defined by the algebraic measure

Definition 7.1 *The* **average crossing number** $\bar{C}$ *is given by the total number of apparent un-signed crossings of the tangle, averaged over the whole domain* $\mathcal{D}$. *We have*

$$\bar{C} = <\sum_r |\epsilon_r|>_{\mathcal{D}} \ . \tag{35}$$

Once again, it is computationally convenient to approximate this measure by the algebraic mean taken over the three principal orthogonal planes, hence

$$\bar{C}_\perp = <\sum_r |\epsilon_r| >_\perp \approx \bar{C} \ . \tag{36}$$

Recent work done by Barenghi, Ricca & Samuels [5] shows that $\bar{C}_\perp$ provides indeed a good approximation to $\bar{C}$ and it seems very effective to detect structural complexity.

Finally, it is of fundamental importance to relate measures of algebraic, geometric and topological complexity to physical properties of the system, such as kinetic helicity and energy. To this end it may be convenient to rewrite eq. (28) in compact form. Consider the linking numbers Lk_{ij} $(i,j \in [1,\ldots,n]$; $Lk_{ii} \equiv Lk_i)$ as elements of a square matrix $(n \times n)$; since $Lk_{ij} = Lk_{ji}$, we can reduce the linking matrix to diagonal form

$$\begin{pmatrix} Lk_{11} & Lk_{12} & \ldots & Lk_{1n} \\ Lk_{21} & Lk_{22} & \ldots & Lk_{2n} \\ \ldots & \ldots & \ldots & \ldots \\ Lk_{n1} & Lk_{n2} & \ldots & Lk_{nn} \end{pmatrix} \rightarrow \begin{pmatrix} M_{11} & 0 & \ldots & 0 \\ 0 & M_{22} & \ldots & 0 \\ \ldots & \ldots & \ldots & \ldots \\ 0 & 0 & \ldots & M_{nn} \end{pmatrix}$$

where each element M_{ii} takes into account self- and mutual linking of the vortex lines. We can therefore re-cast eq. (28) in the form

$$H(\mathcal{L}_v) = \sum_{i=1,\ldots,n} M_{ii}\, f(\kappa) \ , \tag{37}$$

where $f(\kappa)$ is a linear function of quadratic terms of the vortex circulations.

If the tangle is made of vortex filaments of roughly same length L (obtained by an average measure over the tropicity domain $\mathcal{D}$), we can show that on dimensional grounds the enstrophy Θ of the system is given by a relationship of the form

$$\Theta = \int_{\mathcal{D}} |\boldsymbol{\omega}|^2 \, d^3\mathbf{x} = \frac{1}{L} \sum_{i=1,\ldots,n} M_{ii}\, f(\kappa) \ , \tag{38}$$

that provides an interesting connection with helicity. In steady state conditions we can expect to find bounds for minimum enstrophy levels or for other types of 'ground state energies' in relation to the complexity of the physical system.

A combination of algebraic, geometric and topological measures together with kinetic helicity and energy measures provide indeed useful tools to explore complexity and relate flow complexity to energy levels. Work in this direction is in progress.

Acknowledgements

I would like to acknowledge the hospitality of the Isaac Newton Institute for Mathematical Sciences (Cambridge, UK) during the period August–December, 2000. Financial support from UK EPSRC (Grant GR/K99015) is also kindly acknowledged.

References

1. Abraham, R., Marsden, J. & Ratiu, T. (1988) *Manifolds, Tensor Analysis, and Applications.* Springer-Verlag, Berlin.
2. Aref, H. & Zawadzki, I. (1991) Linking of vortex rings. *Nature* **354**, 50–53.
3. Arnold, V.I. (1966) Sur la géométrie différentielle des groupes de Lie de dimension infinie et ses applications à l'hydrodynamique des fluides parfais. *Ann. Inst. Fourier* (Grenoble) **16**, 319–361.
4. Arnold, V.I. & Khesin, B.A. (1998) *Topological Methods in Hydrodynamics.* Applied Mathematical Sciences **125**, Springer-Verlag, New York.
5. Barenghi, C.F., Ricca, R.L. & Samuels, D.C. (2001) How tangled is a tangle? *Physica* D **157**, 197–206.
6. Batchelor, G.K. (1967) *An Introduction to Fluid Mechanics.* Cambridge University Press.
7. Berger, M.A. (1990) Third order link invariants. *J. Phys. A: Math. & Gen.* **23**, 2787–2793.
8. Berger, M.A. & Field, G.B. (1984) The topological properties of magnetic helicity. *J. Fluid Mech.* **147**, 133–148.
9. Ebin, D.G. & Marsden, J.E. (1970) Groups of diffeomorphisms and the motion of an incompressible fluid. *Ann. Math.* **92**, 102–163.
10. Flanders, H. (1963) *Differential Forms with Applications to the Physical Sciences.* Academic Press.
11. Fukumoto Y. & Miyazaki, T. (1991) Three-dimensional distortions of a vortex filament with axial velocity. *J. Fluid Mech.* **222**, 369–416.
12. Hasimoto, H. (1972) A soliton on a vortex filament. *J. Fluid Mech.* **51**, 477–485.
13. Holm, D.D., Marsden, J.E. & Ratiu, T.S. (1998) Euler-Poincaré models of ideal fluids with nonlinear dispersion. *Phys. Rev. Lett.* **80**, 4173–4177.
14. Keener, J.P. (1990) Knotted vortex filaments in an ideal fluid. *J. Fluid Mech.* **211**, 629–651.
15. Kida, S. (1981) A vortex filament moving without change of form. *J. Fluid Mech.* **112**, 397–409.
16. Kida, S. & Takaoka, M. (1988) Reconnection of vortex tubes. *Fluid Dyn. Res.* **3**, 257–261.
17. Langer, J. & Perline, R. (1991) Poisson geometry of the filament equation. *J. Nonlin. Sci.* **1**, 71–93.
18. Moffatt, H.K. (1969) The degree of knottedness of tangled vortex lines. *J. Fluid Mech.* **35**, 117–129.
19. Moffatt, H.K. (1990) The energy spectrum of knots and links. *Nature* **347**, 367–369.
20. Moffatt, H.K. & Ricca, R.L. (1992) Helicity and the Călugăreanu invariant. *Proc. R. Soc. Lond.* A **439**, 411–429.
21. Moffatt, H.K. & Tsinober, A. (1992) Helicity in laminar and turbulent flow. *Annu. Rev. Fluid Mech.* **24**, 281–312.
22. Nakayama, K., Segur, H. & Wadati, M. (1992) Integrability and the motion of curves. *Phys. Rev. Lett.* **69**, 2603–2606.
23. Ricca, R.L. (1991) Intrinsic equations for the kinematics of a classical vortex string in higher dimensions. *Phys. Rev.* A **43**, 4281–4288.

24. Ricca, R.L. (1992) Physical interpretation of certain invariants for vortex filament motion under LIA. *Phys. Fluids.* A **4**, 938–944.
25. Ricca, R.L. (1993) Torus knots and polynomial invariants for a class of soliton equations. *Chaos* **3**, 83–91 [(1995) Erratum. *Chaos* **5**, 346].
26. Ricca, R.L. (1996) The contributions of Da Rios and Levi-Civita to asymptotic potential theory and vortex filament dynamics. *Fluid Dyn. Res.* **18**, 245–268.
27. Ricca, R.L. (2000) Towards a complexity measure theory for vortex tangles. In *Knots in Hellas '98* (ed. McA. Gordon *et al.*), pp. 361–379. Series on Knots and Everything **24**, World Scientific, Singapore.
28. Ricca, R.L. & Berger, M.A. (1996) Topological ideas and fluid mechanics. *Phys. Today* **49** (12), 24–30.
29. Ricca, R.L., Samuels, D.C. & Barenghi, C.F. (1999) Evolution of vortex knots. *J. Fluid Mech.* **391**, 29–44.
30. Saffman, P.G. (1992) *Vortex Dynamics.* Cambridge University Press.
31. She, Z.-S., Jackson, E. & Orszag, S.A. (1990) Intermittent vortex structures in homogeneous isotropic turbulence. *Nature* **344**, 226–228.
32. Shkoller, S. (1998) Geometry and curvature of diffeomorphism groups with H_1 metric and mean hydrodynamics. *J. Funct. Anal.* **160**, 337–365.
33. Thomson, J.J. (1883) *A Treatise on the Motion of Vortex Rings.* Macmillan & Co., London.
34. Tur, A. & Yanovsky, V. (1993) Invariants in dissipationless hydrodynamic media. *J. Fluid Mech.* **248**, 67–106.